Signature of Strong Spin-Orbital Coupling in the Large Nonsaturating Magnetoresistance Material WTe_2

J. Jiang,[1,2] F. Tang,[3] X. C. Pan,[3] H. M. Liu,[3] X. H. Niu,[1,2] Y. X. Wang,[1,2] D. F. Xu,[1,2] H. F. Yang,[4] B. P. Xie,[1,2] F. Q. Song,[3] P. Dudin,[5] T. K. Kim,[5] M. Hoesch,[5] P. Kumar Das,[6,7] I. Vobornik,[6] X. G. Wan,[3,*] and D. L. Feng[1,2,†]

[1]*State Key Laboratory of Surface Physics, Department of Physics, and Advanced Materials Laboratory, Fudan University, Shanghai 200433, China*

[2]*Collaborative Innovation Center of Advanced Microstructures, Fudan University, Shanghai 200433, China*

[3]*National Laboratory of Solid State Microstructures, Collaborative Innovation Center of Advanced Microstructures, and College of Physics, Nanjing University, Nanjing 210093, People's Republic of China*

[4]*State Key Laboratory of Functional Materials for Informatics, Shanghai Institute of Microsystem and Information Technology (SIMIT), Chinese Academy of Sciences, Shanghai 200050, China*

[5]*Diamond Light Source, Harwell Campus, Didcot OX11 0DE, United Kingdom*

[6]*CNR-IOM, TASC Laboratory AREA Science Park-Basovizza, 34149 Trieste, Italy*

[7]*International Centre for Theoretical Physics, Strada Costiera 11, 34100 Trieste, Italy*

(Received 2 April 2015; revised manuscript received 16 June 2015; published 12 October 2015)

We report the detailed electronic structure of WTe_2 by high resolution angle-resolved photoemission spectroscopy. We resolved a rather complicated Fermi surface of WTe_2. Specifically, there are in total nine Fermi pockets, including one hole pocket at the Brillouin zone center Γ, and two hole pockets and two electron pockets on each side of Γ along the Γ-X direction. Remarkably, we have observed circular dichroism in our photoemission spectra, which suggests that the orbital angular momentum exhibits a rich texture at various sections of the Fermi surface. This is further confirmed by our density-functional-theory calculations, where the spin texture is qualitatively reproduced as the conjugate consequence of spin-orbital coupling. Since the spin texture would forbid backscatterings that are directly involved in the resistivity, our data suggest that the spin-orbit coupling and the related spin and orbital angular momentum textures may play an important role in the anomalously large magnetoresistance of WTe_2. Furthermore, the large differences among spin textures calculated for magnetic fields along the in-plane and out-of-plane directions also provide a natural explanation of the large field-direction dependence on the magnetoresistance.

DOI: 10.1103/PhysRevLett.115.166601 PACS numbers: 72.15.Gd, 71.15.Mb, 71.20.Be, 79.60.Bm

The magnetoresistance (MR) of a material reflects the dynamics of the charge carriers and the characteristics of the Fermi surface, and it is useful for magnetic memory and spintronics devices [1,2]. Normally, MR varies as B^2 under low fields, and saturates under high fields. However, anomalously large MR has been discovered in some nonmagnetic materials, such as Ag_2Te/Se [3,4], Bi [5,6], Bi_2Te [7], Cd_3As_2 [8], WTe_2 and $NdSb_2$ [9,10]. MR is often very complicated, involving various factors, and there are several possible mechanisms for these exotic MR behaviors. For example, the large linear MR in Bi_2Te_3 and Bi_2Se_3 is attributed to the quantum limit of the Dirac fermions; namely, all the carriers are situated in the first Landau level [11]. For both Bi and $PtSn_4$, the large MR is attributed to the equal amount of electrons and hole [5,12]. Intriguingly, the large MR in the Dirac semimetal Cd_3As_2 is attributed to a certain protection mechanism that strongly suppresses backscattering in zero field; such a mechanism would be progressively invalidated by the presence of magnetic field, thus causing large MR [8].

WTe_2 was recently reported to exhibit extremely large MR, which shows no signature of saturation up to 60 T [9]. Such an exotic behavior was explained in the framework of Fermi surface compensation [9]. Consistently, angle-resolved photoemission spectroscopy (ARPES) did observe one electron and one hole Fermi pocket with equal area on each side of the Brillouin zone (BZ) center Γ [13]. Further evidence comes from the drastically reduced MR with increased pressure up to 23.6 kPa, accompanied by the increasing size difference between the electron and hole pockets as observed in the Subnikov–de Hass oscillation experiments [14].

Considering the complexity of MR, in this Letter we examine other factors that may contribute to the anomalous MR behavior of WTe_2. Our ARPES data of WTe_2 contain nine Fermi pockets. We found a remarkable photoemission intensity inversion between the right-circularly polarized (RCP) and left-circularly polarized (LCP) light data. Such a circular dichroism (CD) suggests that the orbital angular momentum (OAM) varies with Fermi momentum, an evidence for the presence of strong spin-orbital coupling (SOC). This is further confirmed qualitatively by our band calculations, where the spin texture is observed, as in topological insulators [15,16]. The observed opposite

OAM and spin direction on the opposite side of Γ would provide a mechanism to protect backscattering in zero field. Under a magnetic field, such a mechanism would be compromised, and, thus, affects the resistivity. Moreover, our calculations found that the Fermi surface is almost independent of magnetic field, while the spin textures under magnetic fields along the in-plane and out-of-plane directions exhibit a large difference, which provides a natural explanation of the large field-direction dependence of the MR. Therefore, as suggested in the case of Cd_3As_2 [8], such SOC-induced effects may play a critical role in the large nonsaturating MR of WTe_2.

High-quality WTe_2 single crystals were synthesized by a chemical vapor transport method as reported elsewhere [17]. The in-house ARPES measurements were performed with a SPECS UVLS discharge lamp (21.2 eV He-Iα light) and a Scienta R4000 electron analyzer. The synchrotron ARPES measurements were performed at the I05 beam line of Diamond Light Source equipped with a Scienta R4000 electron analyzer and at the APE beam line of Elettra Synchrotron Trieste equipped with a Scienta DA30 electron analyzer. The angular resolution was 0.3° and the overall energy resolution was better than 15 meV, depending on different photon energies and beam lines. The samples were cleaved *in situ* along the (001) plane and measured under ultrahigh vacuum below 5×10^{-10} torr.

The electronic structure calculations have been carried out using the WIEN2K code with a full potential linearized augmented plane wave method, together with the Perdew-Burke-Ernzerhof parametrization of the generalized gradient approximation as the exchange-correlation functional [18,19]. The basic functions are expanded to $R_{\mathrm{mt}}K_{\mathrm{max}} = 7$ (where R_{mt} is the smallest of the muffin-tin sphere radii and K_{max} is the largest reciprocal lattice vector used in the plane-wave expansion) and the BZ was sampled by 10 000 k points. Using the second-order variational procedure, we include the SOC interaction.

WTe_2 shares a layered structure as do other transition-metal dichalcogenides, but with an additional structural distortion [Fig. 1(a)]. Its space group is P_{mn21} and lacks inversion symmetry. The tungsten chains form the a axis. The BZ of WTe_2 is plotted in Fig. 1(b), where the tungsten chain direction defines Γ-X. The temperature dependent resistivity from 2 to 300 K is plotted in Fig. 1(c), giving a residual resistivity ratio around 58. Although this is lower than that from a previous report [9], the MR of our sample still shows no signature of saturation with a value of 5000% at 2 K under 9 T, as shown in Fig. 1(d). More data of the large nonsaturating behavior at higher magnetic field of our samples can be found elsewhere [20].

The large-scale electronic structure of WTe_2 along Γ-X and Γ-Y are shown in Figs. 2(a) and 2(b), respectively. These bands are mainly contributed by the W 5d orbital and Te 5p orbital [21]. The band structure shows strong anisotropy along Γ-X and Γ-Y, which are more obvious

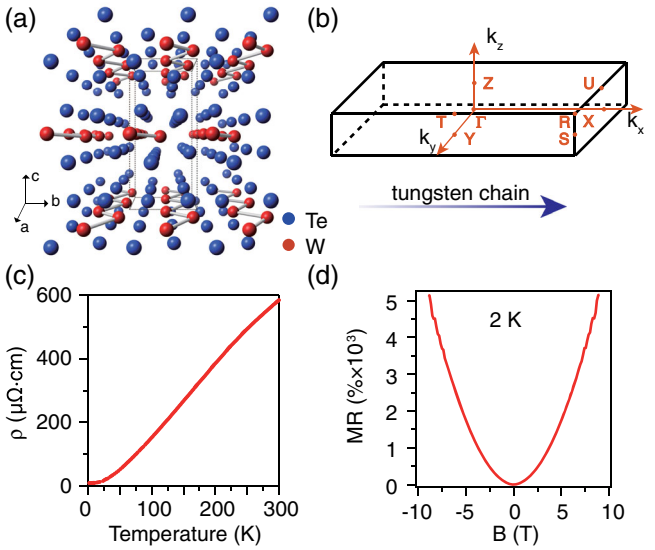

FIG. 1 (color online). (a) Crystal structure of WTe_2, showing the layered structure. The blue and red spheres refer to the Te and W atoms, respectively. (b) Three-dimensional BZ of WTe_2. The high-symmetry points are indicated. (c) Temperature-dependent resistivity of WTe_2 measured from 2 to 300 K. (d) The MR of WTe_2 up to 9 T at 2 K.

in the polarization-dependent data of the Fermi surface mapping presented in Figs. 2(c) and 2(d). There is a hole pocket around Γ, four hole pockets and four electron pockets are resolved along Γ-X, as summarized in Fig. 2(e).

The photoemission intensity plots along cut 2 and cut 3 are shown in Figs. 3(b) and 3(c), respectively. The two electron bands are degenerate at Fermi energy (E_F) across cut 3, but we can distinguish them from the corresponding energy distribution curve (EDC) in Fig. 3(c). The band structure along Γ-X is rather complicated, as shown in Fig. 3(d), together with its second derivative spectrum shown in Fig. 3(e). The corresponding momentum distribution curves (MDCs) and EDCs are shown in Figs. 3(f) and 3(g), respectively. There are in total four bands across the Fermi level, referred to as α, β, γ, and δ. The α band totally contributes three Fermi crossings along Γ-X, crossing 1, 2, and 5, as indicated in Fig. 3(h), which forms the two hole pockets. The β band gives two Fermi crossings indicated as crossing 3 and crossing 4, which forms the other hole pocket. The two electron bands, δ and γ, cross below E_F with Fermi crossings marked as crossing 6 to 9, which form the two electron Fermi pockets shown in Fig. 2(e). There are two bands located around −60 meV (η) and around −185 meV (ζ).

The low-lying electronic structure observed along Γ-X is summarized in Fig. 3(i), giving a better understanding of the four frequencies observed in the quantum oscillations data [14]. We did not observe obvious k_z dependence in our data [see Supplemental Material (SM)], which is different from the calculations and quantum magnetoresistance data [9,24]. This discrepancy might be due to the small k_F's,

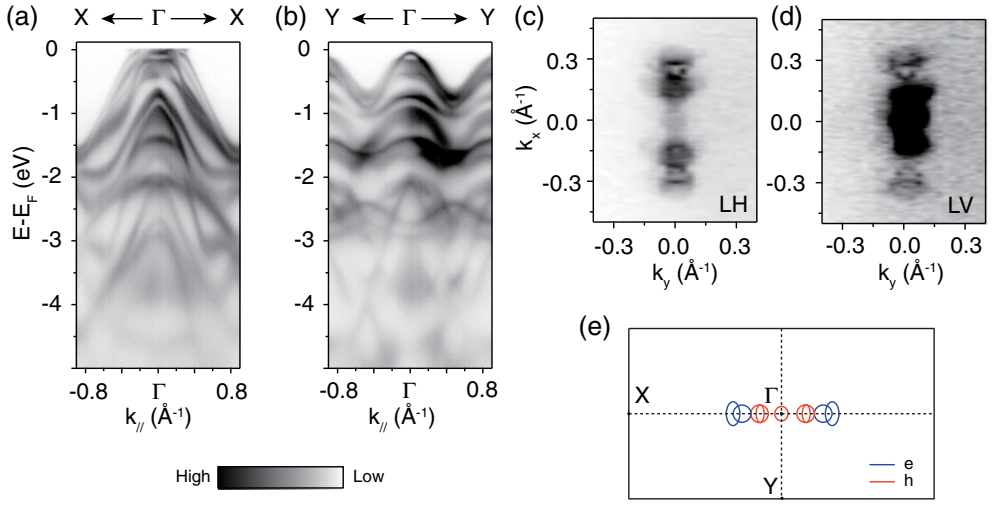

FIG. 2 (color online). (a),(b) Large-scale band structures along Γ-X and Γ-Y, respectively. (c),(d) Fermi surface mapping under linear-horizontal (LH) and linear-vertical (LV) polarized light, respectively. (e) Schematic of the Fermi surface, where the red lines indicate the hole pockets and the blue lines indicate the electron pockets. Data were taken at 7 K with 58 eV photons.

whose variations are beyond the relatively poor k_z resolution of our experiments using vacuum ultraviolet photons. Taking the measured k_F's as k_z-averaged ones, we roughly estimate the ratio of the hole and electron pockets to be around 89%.

It has been shown that the OAM of an electronic state would manifest itself in the CD of ARPES spectra, which is proportional to the inner product between OAM and light propagation vector [16]. Particularly, when strong SOC is present, both OAM and the spin angular momentum of a

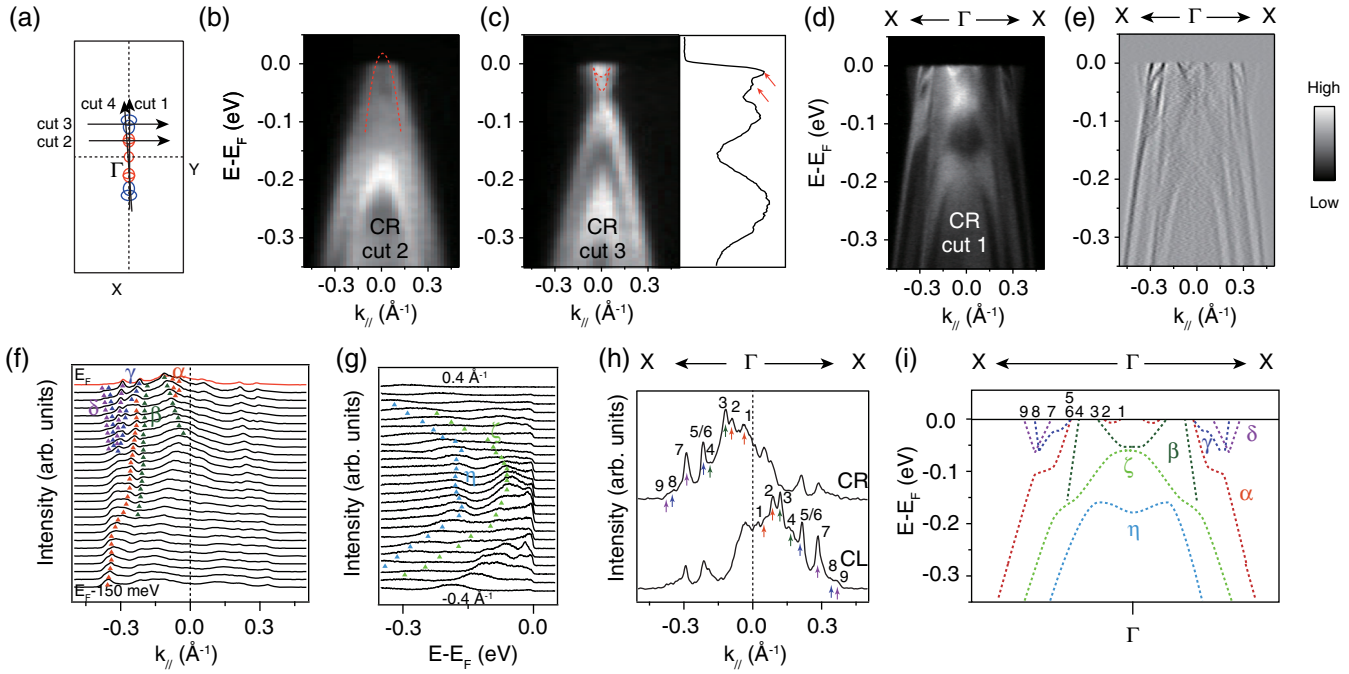

FIG. 3 (color online). (a) Schematic of the Fermi surface of WTe_2. Different cut directions are indicated by the black arrows. (b) The photoemission intensity plot along cut 2. The red dashed line indicates the dispersion of the hole band. (c) Left: The photoemission intensity plot along cut 3. The red dashed lines indicate the dispersion of the electron bands. Right: The corresponding EDC, where the two red arrows highlight the band bottom of the two electron bands. (d),(e) Photoemission intensity plot along Γ-X together with its corresponding second derivative spectrum. (f) The corresponding MDCs of the spectrum in (d) in an energy window [E_F − 150 meV, E_F]. (g) The corresponding EDCs of the spectrum in (d) in a momentum window [−0.4 Å^{-1}, 0.4 Å^{-1}]. (h) MDCs at E_F under RCP light and LCP light, respectively. (i) Schematic of the low-lying electronic structure of WTe_2. Data were taken at 7 K with 58 eV photons.

state would exhibit conjugate textures around the Fermi surface. Consequently, the CD-ARPES technique is a powerful tool to investigate the OAM textures of the surface states in topological insulators, which are manifested as chiral patterns in their CD-ARPES data [15,16,25].

Figure 4(a) shows the Fermi surface mapping of the difference under the RCP and LCP light, namely, RCP-LCP. [The normalized (RCP-LCP)/(RCP + LCP) data can be found in the SM [22]]. The photoemission intensity presents a strong intensity inversion between RCP and LCP data, which is most likely due to different OAM. This can be further confirmed by the corresponding photoemission intensity plot along Γ-X in Fig. 4(b). To understand this, we have performed density-function-theory calculations which give the band structure in Fig. 4(c) and the spin structure on the Fermi surface with $k_z = 0$ in Fig. 4(d). The calculated bands have one-to-one correspondence with the measured ones in Fig. 3(i), as shown by our detailed analysis in the SM, considering that the calculated bands are nearly twofold degenerate [22]. The SOC-induced split between the nearly degenerate bands has an average value of about 15 meV at E_F in the calculation. However, this is not resolved experimentally, likely due to the smaller split caused by renormalization and finite spectral line shape. The antisymmetric spin orientation with respect to Γ can well explain our CD data, which further support that the observed CD is an intrinsic bulk property and not due to some surface effects [26]. Moreover, we note that the spin texture shown in Fig. 4(d) is different from the chiral spin structure in the surface states of a topological insulator [27], though there is a proposal that the metastable 1T' structure of WTe_2 might possess a topological nontrivial state [28]. In fact, during the calculation, we have noticed that the calculated electronic structure is extremely sensitive to the atomic coordinates. Consequently, a quantitative reproduction of the measured electronic structure is still in progress. Nevertheless, we emphasize that the strong SOC effects and spin texture are always present in the calculations.

The opposite spin and OAM textures with respect to Γ would suppress the backscattering channel of the quasiparticles, and, thus, reduce the resistivity. Moreover, in addition to the time-reversal symmetry, the σ_{yz}, σ_{zx}, and c_{2z} lattice symmetry in WTe_2 also give a strong constraint on the spin structure, which consequently forbid several scattering channels (see the SM [22]). Thus, an external field, which changes the spin structure and lifts the scattering protection, will definitely induce a large MR, as discussed in the case of Cd_3As_2 [8].

Inspired by the fact that the MR with magnetic field along z is 10–100 times larger than that with field along

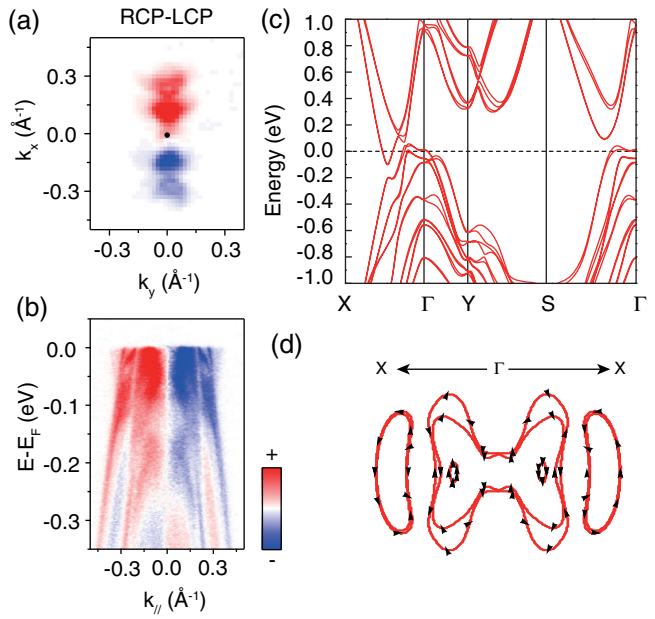

FIG. 4 (color online). (a) The difference of the Fermi surface map measured under RCP and LCP light. The intensity was integrated over a window of $[E_F - 10\ \text{meV},\ E_F + 10\ \text{meV}]$. (b) The corresponding intensity plot along the Γ-X direction. (c), (d) Density-functional calculation of the electronic structure and spin structure at E_F. ARPES data were taken at 7 K with 58 eV photons.

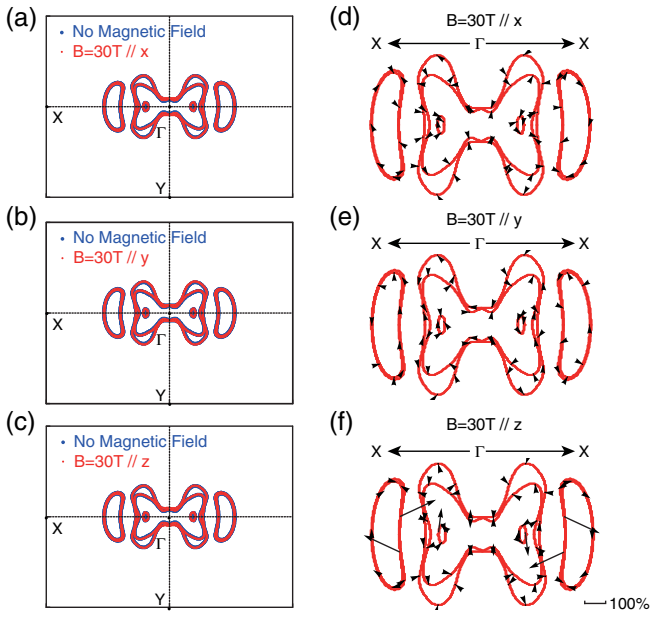

FIG. 5 (color online). (a)–(c) Comparison of Fermi surface at zero field (blue line) and 30 T external magnetic field (red line), along x, y, and z, respectively. (d)–(f) The change of the spin texture induced by the external magnetic field, along x, y, and z, respectively. The relative change of the spin [defined as $[S(30\text{T}) - S(0\text{T})]/S(0\text{T})$] is presented with the black arrow, and the bar in (f) indicates a 100% relative change. To account for external magnetic field, an additional orbital-dependent potential is added in the simple form of $V_{B\text{ext}} = \mu_B \vec{B}_{\text{ext}}(\vec{l} + 2\vec{s})$, where $\vec{l}$ and $\vec{s}$ represent OAM and spin, respectively.

x/y [9], we performed additional calculations of both the Fermi surface and spin structure under magnetic field along the in-plane x axis, y axis, and the out-of-plane z axis in Fig. 5. The external magnetic field has negligible effects on the Fermi surface [Figs. 5(a)–5(c)], but it obviously changes the spin texture [Figs. 5(d)–5(f)]. Particularly, the magnetic field along z has a much larger effect on the spin structure compared with the magnetic fields along x/y. This not only well explains the large MR difference for different field directions, but also further illucidates that the exotic spin texture plays an important role in determining the MR of WTe_2. On the other hand, since the ratio of the populations of the holes and electrons is about 0.89, the electrons and holes are nearly the same within our experimental error bar, our findings may suggest that both mechanisms may contribute to the anomalously large nonsaturating MR of WTe_2.

In conclusion, we presented the comprehensive electronic structure of WTe_2. Particularly, the strong CD indicated an exotic spin structure of this material, which is further confirmed by our band calculations. Our results suggest that in addition to the electron-hole compensation reported earlier, spin-orbital coupling may also play an important role in determining the MR of WTe_2, which would facilitate a more comprehensive understanding of the MR in WTe_2.

We acknowledge helpful discussion with Professor Shiyan Li at Fudan University. This work is supported in part by the National Science Foundation of China under Grants No. 91421109 and No. 11374137 and National Basic Research Program of China (973 Program) under the Grants No. 2012CB921402, No. 2011CB921802, No. 2011CBA00112, and No. 2013CB922103.

Note added.—During the review of this paper, a related study by Wu et al. appeared [29], which reports two pairs of electron pockets and two pairs of hole pockets along the X-Γ-X direction, and a hole-like band around Γ below the Fermi level. This is consistent with our results, except for a slight difference in the chemical potential.

*xgwan@nju.edu.cn
†dlfeng@fudan.edu.cn

[1] A. B. Pippard, *Magnetoresistance in Metals* (Cambridge University, Cambridge, England, 1989).
[2] S. A. Wolf *et al.*, Science **294**, 1488 (2001).
[3] R. Xu, A. Husmann, T. F. Rosenbaum, M.-L. Saboungi, J. E. Enderby, and P. B. Littlewood, Nature (London) **390**, 57 (1997).
[4] M. Lee, T. F. Rosenbaum, M.-L. Saboungi, and H. S. Schnyders, Phys. Rev. Lett. **88**, 066602 (2002).
[5] F. Y. Yang, K. Liu, K. Hong, D. H. Reich, P. C. Searson, and C. L. Chein, Science **284**, 1335 (1999).
[6] F. Y. Yang, K. Liu, K. Hong, D. H. Reich, P. C. Searson, C. L. Chien, Y. Leprince-Wang, K. Yu-Zhang, and K. Han, Phys. Rev. B **61**, 6631 (2000).
[7] D.-X. Qu, Y. S. Hor, J. Xiong, R. J. Cava, and N. P. Ong, Science **329**, 821 (2010).
[8] T. Liang, Q. Gibson, M. N. Ali, M. Liu, R. J. Cava, and N. P. Ong, Nat. Mater. **14**, 280 (2015).
[9] M. N. Ali, J. Xiong, S. Flynn, J. Tao, Q. D. Gibson, L. M. Schoop, T. Liang, N. Haldolaarachchige, M. Hirschberger, N. P. Ong, and R. J. Cava, Nature (London) **514**, 205 (2014).
[10] K. Wang, D. Graf, L. Li, L. Wang, and C. Petrovic, Sci. Rep. **4**, 7328 (2014).
[11] A. A. Abrikosov, Phys. Rev. B **58**, 2788 (1998).
[12] E. Mun, H. Ko, G. J. Miller, G. D. Samolyuk, S. L. Bud'ko, and P. C. Canfield, Phys. Rev. B **85**, 035135 (2012).
[13] I. Pletikosic, M. N. Ali, A. V. Fedorov, R. J. Cava, and T. Valla, Phys. Rev. Lett. **113**, 216601 (2014).
[14] P. L. Cai, J. Hu, L. P. He, J. Pan, X. C. Hong, Z. Zhang, J. Zhang, J. Wei, Z. Q. Mao, and S. Y. Li, Phys. Rev. Lett. **115**, 057202 (2015).
[15] J. Jiang, S. Li, T. Zhang, Z. Sun, F. Chen, Z. R. Ye, M. Xu, Q. Q. Ge, S. Y. Tan, X. H. Niu, M. Xia, B. P. Xie, Y. F. Li, X. H. Chen, H. H. Wen, and D. L. Feng, Nat. Commun. **4**, 3010 (2013).
[16] S. R. Park, J. Han, C. Kim, Y. Y. Koh, C. Kim, H. Lee, H. J. Choi, J. H. Han, K. D. Lee, N. J. Hur, M. Arita, K. Shimada, H. Namatame, and M. Taniguchi, Phys. Rev. Lett. **108**, 046805 (2012).
[17] X. C. Pan, X. L. Chen, H. M. Liu, Y. Q. Feng, F. Q. Song, X. G. Wan, Y. H. Zhou, Z. H. Zhou, Z. H. Chi, Z. R. Yang, B. G. Wang, Y. H. Zhang, and G. H. Wang, Nat. Commun. **6**, 7805 (2015).
[18] P. Blaha, K. Schwarz, G. K. H. Madsen, D. Kvasnicka, and J. Luitz, *WIEN2K* (Technische University Wien, Austria, 2001).
[19] J. P. Perdew, K. Burke, and M. Ernzerhof, Phys. Rev. Lett. **77**, 3865 (1996).
[20] X. C. Pan *et al.* (to be published).
[21] J. Augustin, V. Eyert, Th. Boker, W. Frentrup, H. Dwelk, C. Janowitz, and R. Manzke, Phys. Rev. B **62**, 10812 (2000).
[22] See Supplemental Material at http://link.aps.org/supplemental/10.1103/PhysRevLett.115.166601, which includes Ref. [23], for that explains the different ARPES intensities of different orbitals.
[23] Z. R. Ye, Y. Zhang, F. Chen, M. Xu, J. Jiang, X. H. Niu, C. H. P. Wen, L. Y. Xing, X. C. Wang, C. Q. Jin, B. P. Xie, and D. L. Feng, Phys. Rev. X **4**, 031041 (2014).
[24] L. R. Thoutam, Y. L. Wang, Z. L. Xiao, S. Das, A. Luican-Mayer, R. Divan, G. W. Crabtree, and W. K. Kwok, Phys. Rev. Lett. **115**, 046602 (2015).
[25] Y. H. Wang, D. Hsieh, D. Pilon, L. Fu, D. R. Gardner, Y. S. Lee, and N. Gedik, Phys. Rev. Lett. **107**, 207602 (2011).
[26] J. M. Riley *et al.*, Nat. Phys. **10**, 835 (2014).
[27] M. Z. Hasan and C. L. Kane, Rev. Mod. Phys. **82**, 3045 (2010).
[28] X. F. Qian, J. W. Liu, L. Fu, and J. Li, Science **346**, 1344 (2014).
[29] Y. Wu, N. H. Jo, M. Ochi, L. Huang, D. Mou, S. L. Bud'ko, P. C. Canfield, N. Trivedi, R. Arita, and A. Kaminski, following Letter, Phys. Rev. Lett. **115**, 166602 (2015).